Electrochemiluminescence nanoimmunosensor for CD63 protein using a carbon nanochips/iron oxide/nafion-nanocomposite modified mesoporous carbon interface

Juthi Adhikari[a], Mohammad Rizwan[a,b], Lynn Dennany[c], Minhaz Uddin Ahmed[a*]

[a]*Biosensors and Biotechnology Laboratory, Chemical Science Programme, Faculty of Science, Universiti Brunei Darussalam. Jalan Tungku Link, Gadong, BE 1410, Brunei Darussalam*

[b]*School of Natural Sciences, Bangor University, Bangor, Gwynedd, LL57 2DG, Wales, United Kingdom*

[c]*WESTChem Department of Pure and Applied Chemistry, University of Strathclyde, Technology and Innovation Centre, 99 George Street, Glasgow, G1 1RD, United Kingdom*

[*]*Corresponding author:* minhaz.ahmed@ubd.edu.bn

ABSTRACT

The detection of extracellular vesicles, or exosomes are important mediators in intercellular communication and often play a role in cancer progression. CD63 is a key exosomal protein due to its distinctive cellular functions and association with many cancers. This describes a label-free electrochemiluminescence (ECL) nanoimmunosensor for the detection of CD63 protein over mesoporous carbon screen-printed electrode (MC-SPE) modified with novel nanocomposite of carbon nanochips (CNCs), iron oxide (Fe_3O_4) and nafion (NAF) . Fourier-transform infrared spectroscopy and field emission scanning electron microscopy were used to analyse nanocomposite. All the analytical performance of fabricated CD63 immunosensor were conducted applying ECL. In spite of the simple fabrication strategies utilized, the fabricated immunosensor showcased a broad linear range to detect CD63 from 100 fg mL^{-1} to 10 ng mL^{-1}, with a limit of detection of 100 fg mL^{-1}, excellent selectivity, interference-resistance capability and potential to detect CD63 in real clinical samples.

Keywords: CD63 protein, Electrochemiluminescence, Mesoporous carbon, Carbon nanochips, Immunosensor.

Graphical Abstract

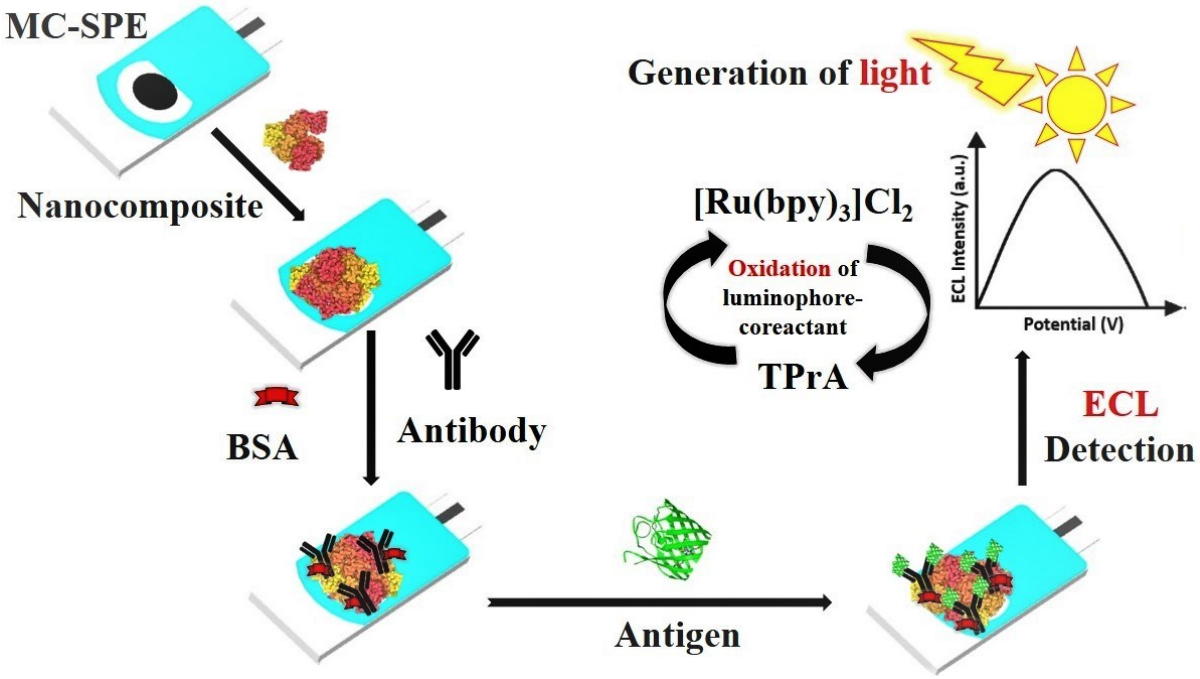

1. Introduction

Exosomes are nano-sized vesicles capable of transferring proteins, DNA, micro-RNA, or lipids with or without direct cell to cell contact representing a novel way of intracellular communication [1]. These exosomes secret specific proteins and nucleic acids that can cause up- and/or down-regulation of physiological processes in respond to local environments often to facilitate tumour angiogenesis and metastasis [1]. As such, these proteins and nucleic acids can be used as novel biomarkers for the detection and diagnosis of several diseases and ailments [2]. Exosomes are produced by most eukaryotes. The sources can vary from different cells (e.g., endothelial cells, mast cell, dendritic cells, platelets, neurons, etc.) to various body fluids, such as saliva, blood, amniotic fluid, urine, breast milk, tears, and sweat in human [3]. Exosomes secret a wide range of proteins including CD63, CD81, CD44, and CD69, to name a few. Among them, CD63 is the most extensively studied due to its correlation to several fatal cancers (e.g. breast cancer, ovarian cancer etc.) [3]. CD63 protein has four distinct hydrophobic domains allowing it to be associated with important cellular functions (i.e. cell development, cell activation and cell motility) [4]. Moreover, the high level of CD63 protein is linked with cervical cancer, melanoma, and pancreatic cancer as well as others [5]. A simple, quick and cost-effective technique to monitor for CD63 is crucial to facilitate the early detection and prognosis of the disorders, in particular cancer diagnosis.

Currently, different methods are available to detect and measure the exosomal protein CD63, such as, sandwich ELISA [6], chemiluminescence [7], flow cytometry [8], western blotting [9]. However, all these techniques require high throughput settings, expert technicians, and are often quite time-consuming from initial sampling to result. Therefore, this study proposes a label-free electrochemiluminescence (ECL) biosensor involving non-hazardous reagents, which will be both highly sensitive and start to develop a more time-efficient process.

Furthermore, we seek to build cheaper materials so that this sensor will also be economically viable.

Lately, ECL has become enormously popular among researchers for its sensitivity and accuracy in obtaining quick and reliable results [10-13]. ECL is an electrochemical process between luminophore and co-reactant which produce light when a specific voltage is applied. Most commonly, the co-reactant ECL pathway is utilised for analytical detection methods [14,15]; this is particularly true for sensors targeting analytes within complex biological matrices highlighting its potential within this field [16,17]. Other advantages of ECL includes the absence of background signal, its flexibility and suitable to many different electrode materials, sizes and dimensions, reaction position, reaction time, as well as control over applied potential and currents [18-20]. Moreover, ECL techniques are incredibly versatile, which makes them easily accessible for modifications with nanoparticles and nanomaterials [21-23].

Different types of electrodes, including screen-printed electrodes (SPE), glassy carbon electrodes (GCE), or disposable electrode printed-chips (DEP-chips) can be used in designing ECL based sensors establishing ECL as both a diverse and versatile analytical detection method [24]. The mechanism of ECL detection within an immunosensor mainly relies upon the interactions of luminophore and the working electrode. The applied voltage causes the luminophore to be oxidised, donating electrons at the electrode surface. However, as the thickness of the antibody-antigen increases over the electrode, the interactions between luminophore and electrode decreases [25]. Further, the ECL intensity may increase and decrease depending on the net charge of the implied biomolecules on the working electrode surface [26].

The trend of incorporating different carbon and metal-based nanoparticles and nanomaterials to enhance immunosensor performance has been exploited in several works [23,

25, 27,]. Within in this work, we have used carbon nanochips (CNCs) and iron oxide (Fe_3O_4) as the core nanomaterials to modify mesoporous carbon screen-printed electrode (MC-SPE) working electrodes. The CNCs are two-dimensional (2D) carbon sheets resembling a similar structure of carbon nanotubes having exceptional mechanical and electrical conductivity [28]. For instance, they not only promote electron transfer on the working electrode but also reduce the rate of biofouling during analysis. In addition, Fe_3O_4 has proven to be extremely versatile for the enhancement of sensor performance [29, 30, 31]. Therefore, CNCs and Fe_3O_4 were chosen to integrate into the nanocomposite. Later, NAF was added to the CNCs/Fe_3O_4 composite to achieve a unique negatively charged engineered nanocomposite (CNCs/Fe_3O_4/NAF) [32, 33]. The main function of the nanocomposite is to facilitate high electron transfer during the ECL reaction. Therefore, CNCs/Fe_3O_4/NAF nanocomposite is expected to attract the positively charged luminophore (tris(2,2′-bipyridyl) dichlororuthenium (II) hexahydrate); $Ru(bpy)_3]Cl_2 \cdot 6H_2O$, over the MC-SPE/CNCs/$Fe_3O_4$/NAF electrode by attractive electrostatic interaction. This enable more electron transfer between the modified electrode surface (MC-SPE/CNCs/Fe_3O_4/NAF) and $[Ru(bpy)_3]^{2+}$/tripropylamine (TPrA) complex via redox reaction providing high ECL signal. The mechanism of the reaction between the luminophore $(Ru(bpy)_3]Cl_2 \cdot 6H_2O$) and the co-reactant (TPrA) and transfer of electrons is shown in scheme 1. Moreover, another fundamental purpose of finding a suitable nanocomposite was to make the nanoimmunosensor highly sensitive, efficient, and stable. $Ru(bpy)_3]Cl_2 \cdot 6H_2O$ was used as the luminophore and TPrA as the co-reactant for the generation of ECL. The paring of these two reagents has been shown to be very useful in terms of obtaining consistent and repeatable ECL signals [25, 34].

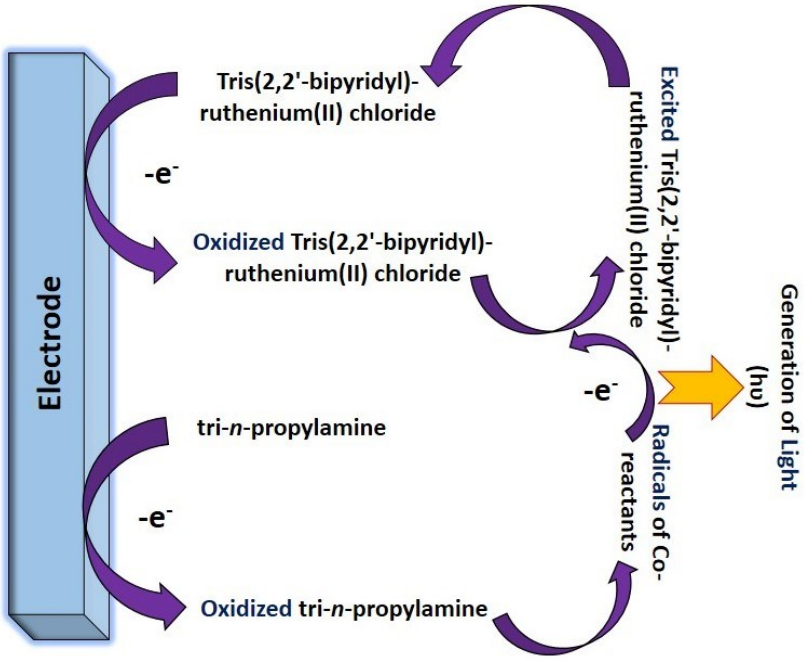

Scheme 1: The mechanism of the reaction between the luminophore and the co-reactant over the electrode and transfer of electrons.

In this study, for the first-time novel CNC nanomaterial was successfully integrated into a nanocomposite to facilitate enhanced ECL for the sensitive detection of the CD63 protein. This fabricated immunosensor (MC-SPE/CNC/Fe_3O_4/NAF/anti-CD63/BSA) showcased notable stability and reproducibility in detecting target protein, CD63 and exhibited a wide linear range 100 fg mL^{-1} to 10 ng mL^{-1} and a low detection limit of 100 fg mL^{-1} for the detection of CD63. This highlight both the potential of these nanomaterials as well as the application of ECL for biomedical applications.

2. Materials and Methods

2.1. Reagents and solutions

Rabbit monoclonal antibody CD63 and exosomal protein CD63, CD81, CD69, bovine serum albumin (BSA), carcino-embryogenic antigen (CEA), alpha fetoprotein (AFP), haptoglobin (Hp), sodium azide, potassium chloride, potassium ferrocyanide, potassium

ferricyanide, tris (2,2′-bipyridyl) dichlororuthenium(II) hexahydrate, tripropylamine, tris-disodium phosphate, and monosodium phosphate, nanocomposite binding agent, carbon nano chips (CNCs), 5% NAF solution were purchased from Sigma-Aldrich (USA). Iron oxide (Fe_3O_4) nanoparticles were procured from US Research Nanomaterials, Inc. (Houston, USA). All solutions were prepared using freshly obtained Milli-Q water (deionised with specific resistance ~18 $M.cm^{-1}$). All the experiments were performed at the room temperature (RT) (21 ± 0.5 °C).

2.2. Instrumentations

All the ECL measurements were performed utilizing an MPI-A capillary electrophoresis electrochemiluminescence analyzer system, purchased from Xi′an Yima Opto-Electrical Technology Co., Ltd. (China). A handmade ECL working cell (height 5 cm, width 1.5 cm) was utilized to detect the light generated from the reactions between ECL probe and the electrode surface. The ECL cell was placed on top of a photomultiplier tube (PMT) which was connected to the MPI-A software to analyse ECL intensity. The fabricated sensor was immersed in the ECL cell containing luminophore-coreactant mixture ($[Ru(bpy)_3]Cl_2$-TPrA) and placed on the PMT to conduct ECL measurement. The electrochemical layer-by-layer characterization studies cyclic voltammetry (CV), chronocoulometry (CC), and electrochemical impedance spectroscopy (EIS) were carried out using Autolab PGSTAT101 III potentiostat/galvanostat (Metrohm, Netherlands) connected to a Nova software version 1.10. The disposable screen-printed electrodes were purchased from DropSens (Spain), where the working electrode was modified with mesoporous carbon, reference electrode with silver, and the counter electrode with carbon. The diameter of the mesoporous carbon modified working electrode was 4 mm. The overall dimensions of these non-reusable ceramic electrodes are (L33 × H0.5 × W10) mm. The surface topographical study was done by using field-emission electron microscopy (FE-

SEM) JEOL, JSM-7610F (Japan). Fourier-transform infrared (FTIR) spectroscopy (Shimadzu, Japan) was used for the analysis of nanocomposite. All experiments were performed at constant room temperature (21±0.5°C) and atmospheric pressure in an air-conditioned laboratory. All experimental data are an average of three replicates achieved from three different fabricated sensors maintaining similar optimal conditions.

2.3. Preparation of CNCs/Fe_3O_4/NAF nanocomposite

The preparation of the selected CNCs/Fe_3O_4/NAF nanocomposite was done in-house at 21±0.5 °C. Briefly, CNCs and Fe_3O_4 were prepared in two separate small glass vials by dissolving in dH_2O and were ultra-sonicated for 3.5 h for uniform dispersion. Next, the sonicated nanoparticles were gradually diluted to achieve the optimum concentrations (10 µg mL^{-1} for CNCs and 20 µg mL^{-1} for Fe_3O_4). In the meantime, 0.25 % NAF was also prepared by serially diluting it using double dH_2O from the main stock. Finally, the synthesis of the final nanocomposite was performed by mixing 10 µg mL^{-1} for CNCs, 20 µg mL^{-1} for Fe_3O_4, and 0.25 % NAF at 1:1 ratio and stirring it at a magnetic stirrer for 6 h. The resulting nanocomposite mixture was stored at 4 ºC and was ultra-sonicated for 60 min before each use.

2.4. ECL Fabrication of the CD63 nanoimmunosensor

Firstly, CNC/Fe_3O_4/NAF nanocomposite was dropped over bare MC-SPE and dried for 2 h to form CNC/Fe_3O_4/NAF nanocomposite modified working electrode MC-SPE (MC-SPE/CNC/Fe_3O_4/NAF). Then, 10 µL of the anti-CD63 solution (1 µg/mL) was spiked over MC-SPE/CNC/Fe_3O_4/NAF and incubated overnight at 4 °C to immobilise onto the electrode surface by chemisorption [35]. Next, MC-SPE/CNC/Fe_3O_4/NAF/anti-CD63 was washed using 10 mM PBS (pH 7.4) to remove loosely bounded antibody and dried at RT. Following washing and drying 0.1 % BSA was spiked over MC-SPE/CNC/Fe_3O_4/NAF/anti-CD63 as the blocking agent to minimize the non-specific binding and formation of MC-SPE/CNC/Fe_3O_4/NAF/anti-

CD63/BSA. Later, MC-SPE/CNC/Fe_3O_4/NAF/anti-CD63/BSA was washed using PBS (pH 7.4) and dried at RT. Finally, the fabricated MC-SPE/CNC/Fe_3O_4/NAF/anti-CD63/BSA nanoimmunosensor was stored at 4 °C until further use. Scheme 2 depicts step-by-step fabrication of the ECL nanoimmunosensors for CD63 detection.

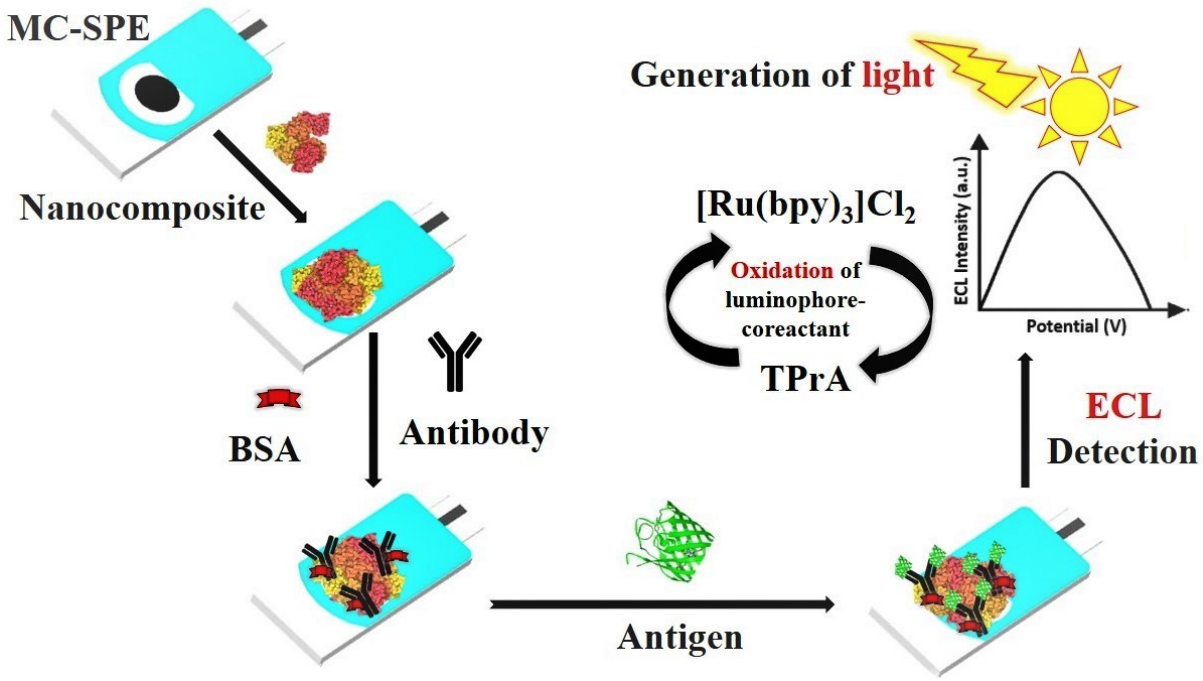

Scheme 2: A diagrammatic arrangement of the of label-free electrochemiluminescence nanoimmunosensor to detect exosomal protein (CD63).

2.5. ECL Detection of CD63

The ECL detection of CD63 was accomplished by applying different concentrations of CD63 on MC-SPE/CNC/Fe_3O_4/NAF/anti-CD63/BSA nanoimmunosensor. To obtain the ECL measurements for each of the CD63 concentrations, 10 µL of CD63 was incubated on nanoimmunosenor for 60 min (at RT 21 ± 0.5°C) followed by washing (with 10 mM PBS, pH 7.4) and drying. The ECL detection was performed by pre-making the ECL probe mixture. The

total volume of the ECL probe was 4 mL containing 1 mL of $[Ru(bpy)_3]^{2+}$ (1 mM) and TPrA (100 mM) each, and 2 mL of10 mM PBS having pH 7.4. The glass cell was entirely covered with aluminium foil paper, only exposing the bottom section (diameter 1.5 cm) to authorize the diffusion of light over the PMT. The ECL cell was kept on top of the PMT which was in a lightproof black box to ensure the maximum performance of the ECL analyser without the disturbance of external light source. All ECL measurements were performed using primary potential of 0.2 V, end potential of 1.25 V and the lowest potential as -0.2 V. The selected scan rate was 100 mV s^{-1} with an amplifying series of 3, sensitivity 1×10^{-6} and PMT potential of 800 V. Maximum ECL intensity was obtained at ~10 seconds after starting each cycle. The error bars signify the relative standard deviations of at least three replicates (n = 3) for all experiments.

3. Results and Discussion

3.1. CNCs/Fe_3O_4 characterization using FTIR:

Composition of CNCs/Fe_3O_4 nanocomposite was analysed using FTIR. 2 mg of the nanocomposite sample was mixed with 200 mg KBr to form a pellet of fine consistency. Figure 1 represents the prominent peak patterns of CNCs (a) and Fe_3O_4 (b) respectively having a wavenumber range between 800 to 4000 cm^{-1} and a transmittance percentage (%) from 0 to 2.5. The major peak differences have been observed between 700 cm^{-1} to 1600 cm^{-1} regions and the percentage of peak transmittance starts from 0.2 % Fe_3O_4 and 1.8 % for CNCs. For CNCs [Fig 1 (a)], peak at 1614.49 cm^{-1} region shows the C=C stretching whereas spectra at 2926.14 cm^{-1} and 2853.81 cm^{-1} exhibited the $–CH_2$ alignment respectively [36]. In the case of Fe_3O_4 [Fig 1 (b)], the peak at 3440.19 cm^{-1} regions signified the O-H stretching group [37]. Additionally, 1642.46 cm^{-1}, 1023.48 cm^{-1} denoted the surface hydroxyl group and nitrate

stretching vibrations whereas peaks at 956.41 cm^{-1} represent the F-O alignment [38]. Thus, the FTIR spectra successfully confirms the presence of CNCs and Fe_3O_4 within the nanocomposite.

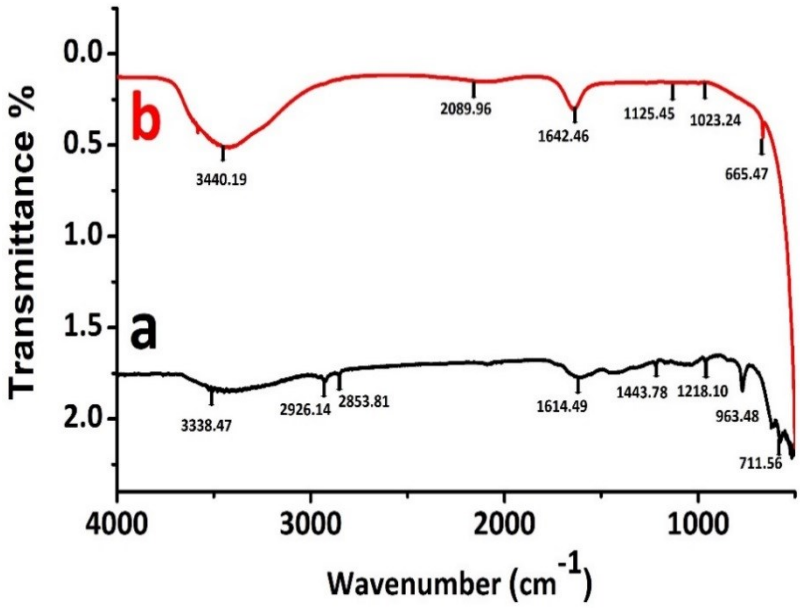

Fig. 1. FTIR spectra of CNCs **(a)**, and Fe_3O_4 **(b)** plotting wavenumber (cm^{-1}) against % of transmittance.

3.2. Microscopic (SEM) characterization of CNCs/Fe_3O_4/NAF nanocomposite

In order to confirm the structure of the nanocomposite layer on MC-SPE, each nanoparticle was tested using FE-SEM. Nanoparticles were individually incubated on MC-SPE (Fig. 2A) and analysed using FE-SEM. CNCs exhibited fibrous-small thread-like structures (Fig. 2B), whereas iron oxide (Fe_3O_4) showed small spherical like orientations (Fig. 2C). In addition, Fig S1A and Fig S1B displayed the nanocomposite layer incubated with antibody and antigen respectively which showcased extremely distinct features *i.e.* in Fig S1A, large assemblies of antibody and BSA was visible. Whilst, in the case of Fig S1B, the big alignments were covered by antigen layer exhibiting a smooth surface possibly due to immunocomplex formation between anti-CD63 and CD63 protein over the nanoimmunosensor.

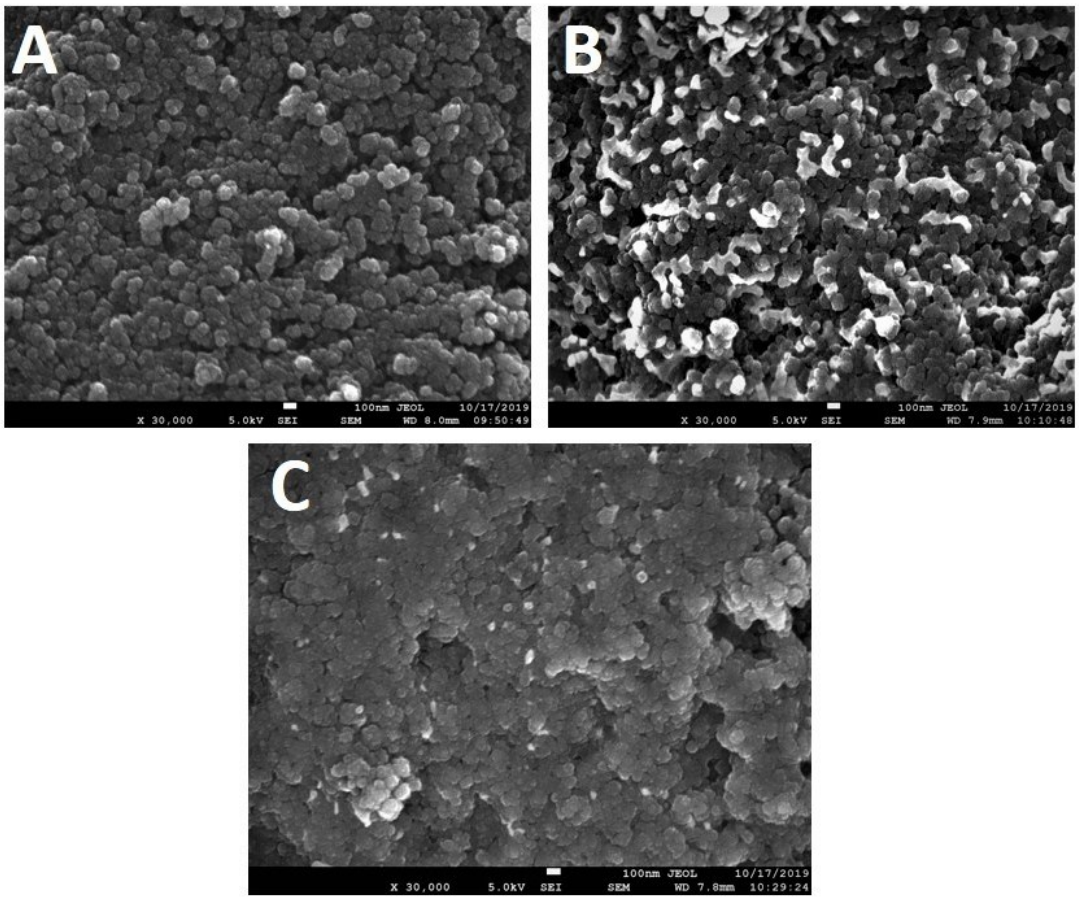

Fig. 2. SEM images: **(A)** MC-SPE; **(B)** CNCs/MC-SPE; and **(C)** Fe_3O_4/MC-SPE at 30,000×.

3.3. ECL characterisation of CNCs/Fe_3O_4/NAF nanocomposite

Further, characterisation of the CNCs/Fe_3O_4/NAF nanocomposite was performed by EC and ECL methods. The ECL produced from each layer of the nanocomposite modified on the surface of the MC-SPE was recorded to investigate the ECL enhancement observed due to the addition of the nanoparticles. The recorded ECL signal for nanoparticle and nanocomposite was compared and plotted against bare MC-SPE (Fig. 3A). There was a large increase in the

ECL intensity of CNCs/Fe_3O_4/NAF nanocomposite modified MC-SPE [Fig. 3A, curve (d)] compare to the bare MC-SPE [Fig. 3A, curve (a)].

3.4. Electrochemical characterisation of the nanocomposite

Following ECL characterisation of nanocomposite layer, the nanocomposite was subjected to electrochemical characterisation, where the nanoparticle and their composite was characterised applying CV based on their response against a constant set of potential. Similar trend was noticed for each layer of the nanoparticles and their composite on electrochemical analysis when compared to ECL. Briefly, after incubating the working electrode with CNCs, there was a significant rise in electrochemical response [Fig. 3B, curve (b)] in comparison with the bare MC-SPE [Fig. 3B, curve (a)]. After the addition of Fe_3O_4, the electrochemical signal was further enhanced due to the highly conductive properties of the iron oxide nanoparticles [Fig. 3B, curve (c)]. And finally, the addition of the nanocomposite (CNCs/Fe_3O_4) on MC-SPE, showcased the maximum electrochemical current observed [Fig. 3B, curve (d)]. CC study was conducted for the MC-SPE [Fig. 3C, bar (a)], CNCs/MC-SPE [Fig. 3C, bar (b)], Fe_3O_4/CNCs/MC-SPE [Fig. 3C, bar (c)], and Fe_3O_4/CNCs/MC-SPE [Fig. 3C, bar (d)]. These results demonstrated a gradual increase in the electrostatic charge in correlation to the ECL and electrochemical study.

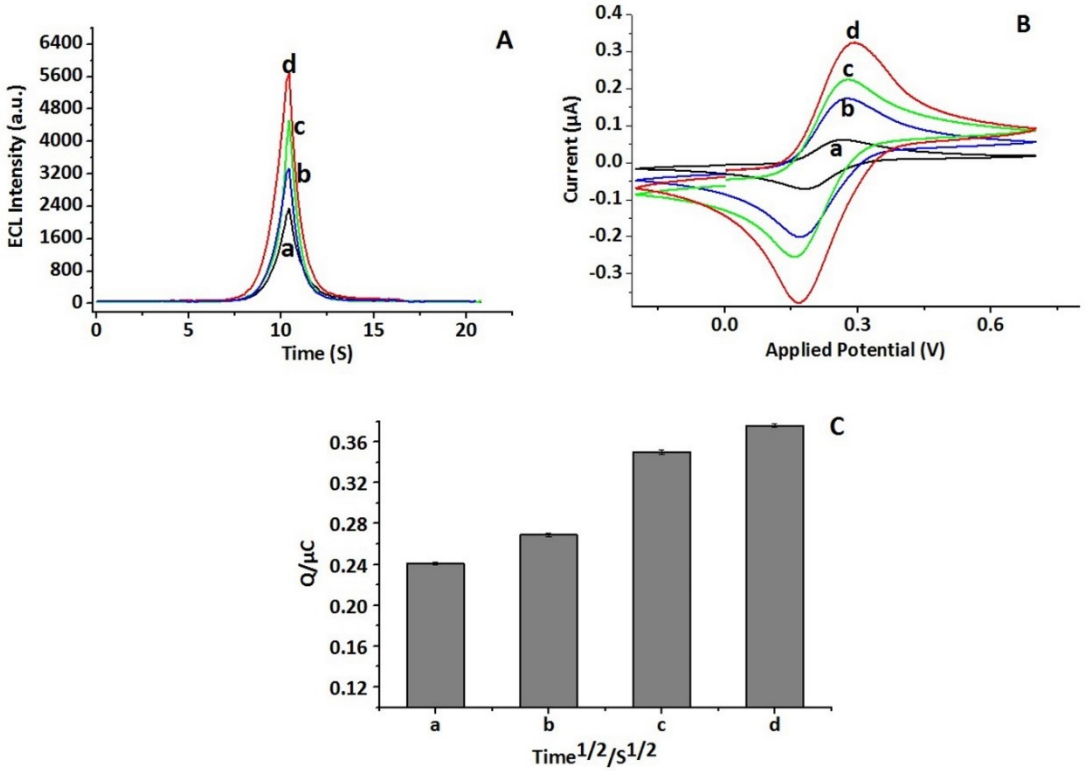

Fig. 3. Characterisation of nanocomposite via ECL, electrochemical and CC techniques: **(A)** ECL intensity graph of **(a)** MC-SPE, **(b)** CNCs/MC-SPE, **(c)** Fe_3O_4/CNCs/MC-SPE, **(d)** NAF/Fe_3O_4/CNCs/MC-SPE; **(B)** Electrochemical graph of **(a)** MC-SPE, **(b)** CNCs/MC-SPE, **(c)** Fe_3O_4/ MC-SPE, **(d)** Fe_3O_4/CNCs/MC-SPE; and **(C)** CC bar diagram of **(a)** MC-SPE, **(b)** CNCs/MC-SPE, **(c)** Fe_3O_4/MC-SPE, **(d)** Fe_3O_4/CNCs/MC-SPE.

3.5. Optimisation of anti-CD63 concentration and immobilization time

The optimisation of antibody (anti-CD63), was accomplished by examining three different concentrations of anti-CD63 (5 μg mL^{-1}, 1 μg mL^{-1} and 0.5 μg mL^{-1}) on the MC-SPE/CNCs/Fe_3O_4/NAF platform at 21±0.5 °C using 100 pg mL^{-1} CD63 as illustrated in Figure 4. Subsequently, 1 μg mL^{-1} was chosen as the optimum working concentration to develop MC-SPE/CNCs/Fe_3O_4/NAF/anti-CD63 nanosensor to capture out target antigen (CD63). Herein, blocking was performed for 60 min, and immune-complex (antibody-antigen) formation time

was 1 h at 21±0.5 °C (Fig. 4B). Following that, the incubation time for CD63 antibody was selected by optimising three distinct periods (3, 6 and 12±1 h) where maximum and stable CV response was measured for 12±1 h incubation of the antibody using 100 pg mL^{-1} CD63. Henceforth, 12±1 h was chosen as the optimum incubation time for anti-CD63 (Fig. 4B). Therefore, within all further analysis blocking was performed for 60 min, and the antigen-antibody reaction was carried out for 1 h at 21±0.5°C in 10 mM PBS, pH 7.4 (n=3).

3.6. Optimisation of blocking by BSA and antibody-antigen reaction time

The selection of the incubation time of blocking agent, BSA was achieved by preparing 0.1 % BSA in 0.1 % NaN_3 in 10 mM PBS (pH 7.4) and 30, 60 and 90 min incubation times were verified to mitigate the nonspecific binding at the surface of MC-SPE/CNCs/Fe_3O_4/NAF/anti-CD63/BSA immunosensor using 100 pg mL^{-1} CD63. The highest ECL peak was recorded at 60 min (Fig. 4C), so 1 h was selected as the optimum blocking time for this immunosensor. Thereafter, to optimise the immunocomplex formation time between anti-CD63 and CD63 protein (100 pg mL^{-1}), three different time (30, 60, and 90 min) were tested on MC-SPE/CNCs/Fe_3O_4/NAF/anti-CD63/BSA nanosensor, where 60 min showcased maximum and repeatable ECL intensity. Henceforth, 1 h was selected as the optimum antibody-antigen reaction time between anti-CD63 and CD63 protein (Fig. 4D) at 21 ± 0.5°C in 10 mM PBS, pH 7.4 (n=3).

3.7. Optimisation of $[Ru(bpy)_3]^{2+}$ and TPrA

For the optimisation of the $[Ru(bpy)_3]^{2+}$, different concentrations (0.5 mM, 1.0 mM and 2.0 mM), of $[Ru(bpy)_3]^{2+}$ were tested and 1 mM $[Ru(bpy)_3]^{2+}$ was found with decent stability and reproducibility. Henceforth, 1 mM $[Ru(bpy)_3]^{2+}$ was chosen as the optimum concentration to combine with tripropylamine (TPrA) (Fig. 4E). Simultaneously, the working concentration

of TPrA was selected after trying three different concentrations (20 mM, 50 mM and 100 mM), where 100 mM of TPrA was found to have superior stability (Fig. 4F). The working ratio of $[Ru(bpy)_3]^{2+}$ and TPrA was chosen as 1:100 [18].

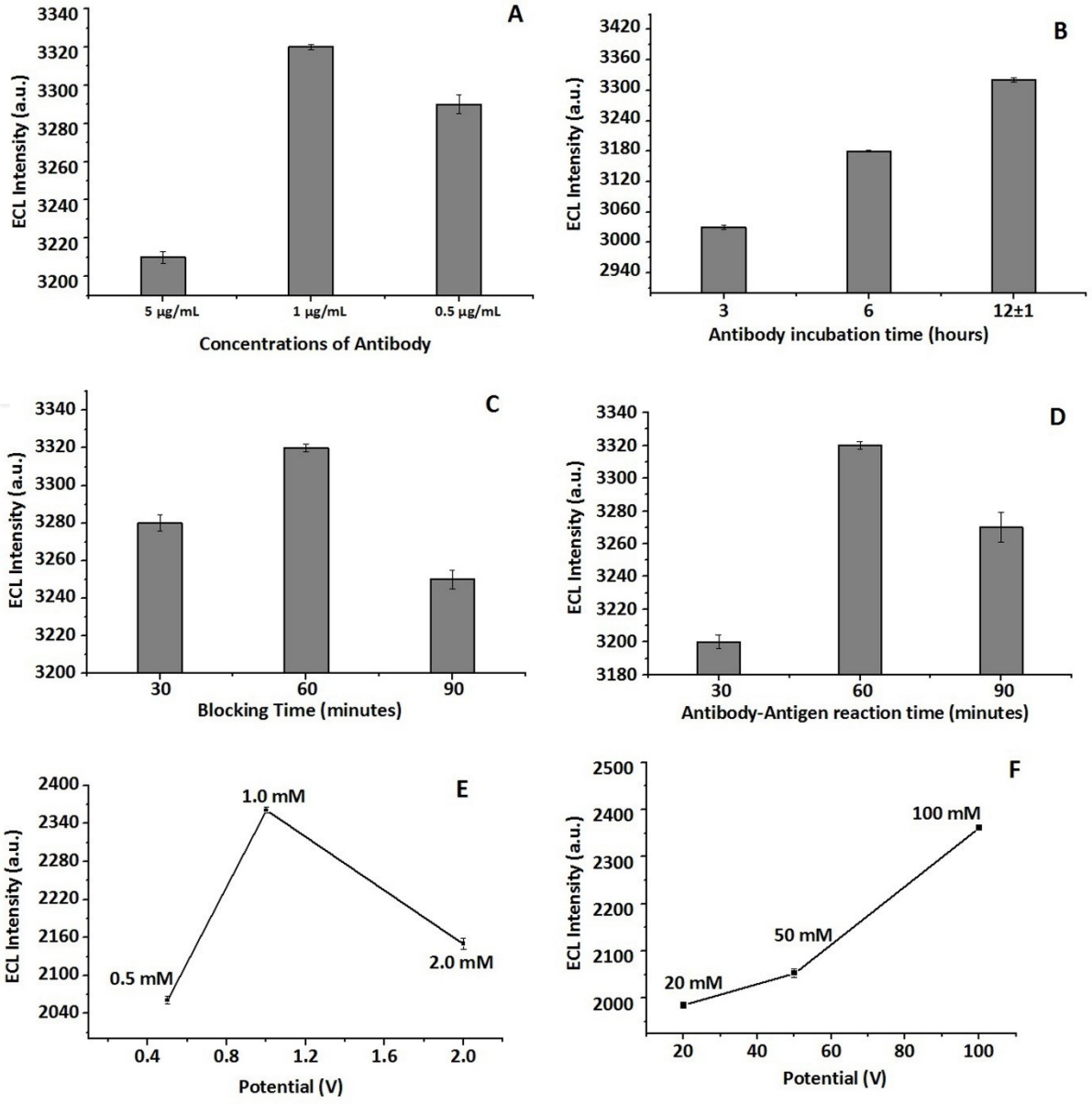

Fig. 4. (A) Optimisation of anti-CD63 working concentration (5 µg mL^{-1}, 1 µg mL^{-1}, and 0.5 µg mL^{-1}) of the anti-CD63, that were spiked on the MC-SPE/CNCs/Fe_3O_4/NAF immunosensor with 100 pg mL^{-1} CD63; **(B)** Optimisation of anti-CD63 (1 µg mL^{-1}) incubation time on MC-SPE/CNCs/Fe_3O_4/NAF platform with 100 pg mL^{-1} CD63; **(C)** Optimisation of the blocking time by 0.1 % BSA in 0.1 % NaN_3 prepared in 10 mM PBS, pH 7.4 spiked on MC-SPE/CNCs/Fe_3O_4/NAF/anti-CD63 for 30, 60 and 90 min with 100 pg mL^{-1} CD63; **(D)** anti-CD63 and CD63 protein reaction were carried out for 30, 60 and 90 min with 100 pg mL^{-1}

CD63 on MC-SPE/CNCs/Fe_3O_4/NAF/anti-CD63/BSA.; **(E)** Optimisation of $[Ru(bpy)_3]^{2+}$ working concentration; and **(F)** Optimisation of TPrA working concentrations. All ECL analysis was performed in the presence of $[Ru(bpy)_3]Cl_2$-TPrA.

3.8. ECL and Electrochemical scan rates study of nanoimmunosensors

Both ECL and electrochemical scan rates study was performed to demonstrates the electrochemical diffusion over nanoimmunosensors. Fig. 5A shows the increase in ECL intensity was related to the increase in scan rates, and the maximum ECL signal was recorded at a scan rate of 100 mV s^{-1}. Whereas, Fig. 5B showcased the oxidation peaks *vs.* square root of scan rates exhibiting a linear relationship between the tested scan rates. Likewise, the diffusion kinetics study was performed using $[Fe(CN)_6]^{3-}$ /$[Fe(CN)_6]^{4-}$ on the nanoimmunosensor surface applying electrochemical diffusion kinetic, at scan rates 20 mVs^{-1} to 100 mV s^{-1}. The linear relationship of the oxidation-reduction peaks and the square root of the scan rate was demonstrated by the nanoimmunosensors respectively in Fig. 5C and D. Further, heights of the peaks increase with the increasing scan rates portray the dependency on electrochemical diffusion supporting the earlier findings [39, 40].

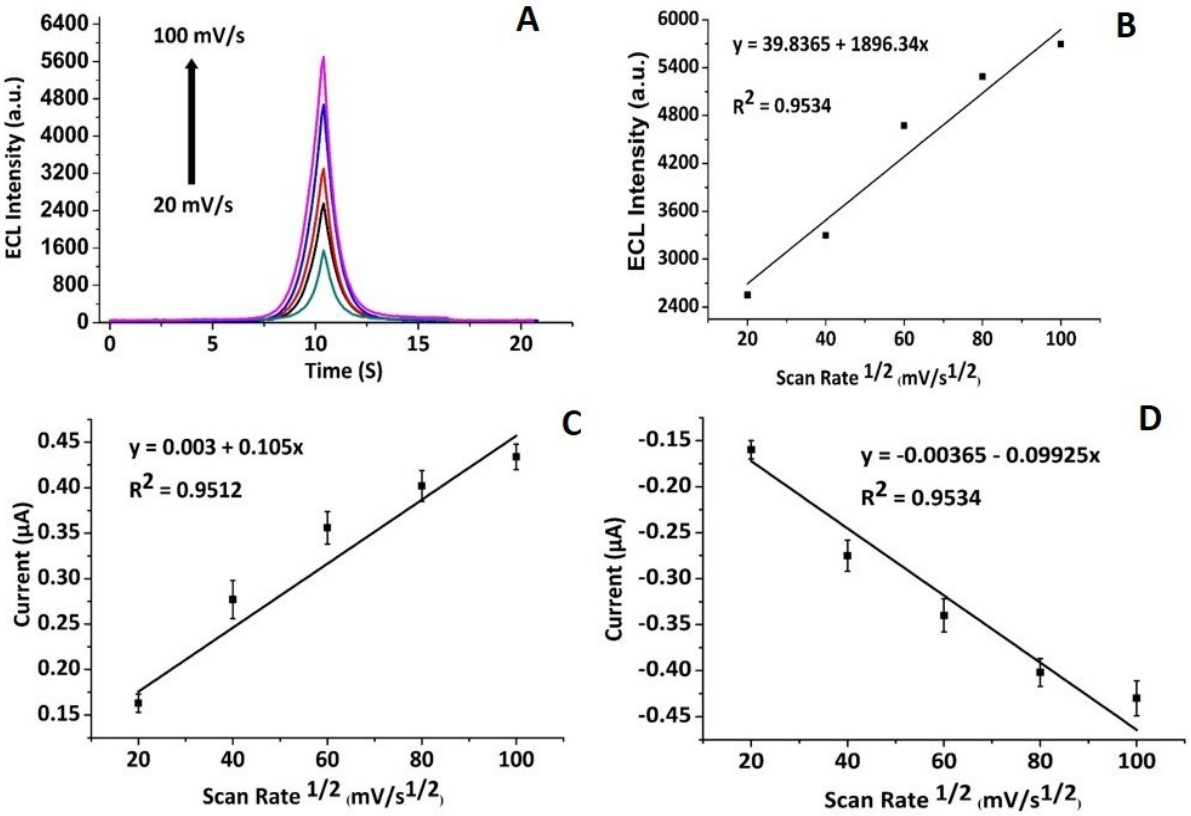

Fig. 5. (A) ECL intensity of the fabricated immunosensor from 20 mV/s to 100 mV/s; **(B)** Dependence of oxidation peak currents on the square root of the scan rates using 1:100 $[Ru(bpy)_3]Cl_2$-TPrA; **(C)** Dependence of oxidation peak currents on the square root of the scan rates; and **(D)** Dependence of reduction peak currents on the square root of the scan rates utilizing 5 mM $[Fe(CN)_6]^{3-}/[Fe(CN)_6]^{4-}$ redox probe.

3.9. ECL and Electrochemical characterisation of MC-SPE/CNCs/Fe_3O_4/NAF/anti-CD63/BSA

For the layer-by-layer ECL characterisation of the MC-SPE/CNCs/Fe_3O_4/NAF/anti-CD63/BSA nanoimmunosensor, each layer was individually incubated, and data were analysed. Firstly, the ECL intensity for the bare MC-SPE was recorded [Fig. 6A, curve (a)]. Thereafter, the ECL intensity was measured after incubating with CNCs/Fe_3O_4/NAF nanocomposite, which exhibited a significant increase in ECL peak signal compared to the bare electrode [Fig. 6A, curve (b)]. The maximum rise in the ECL signal was due to the high

electrochemical conductivity of the nanoparticles (CNCs, Fe_3O_4) used in preparing the nanocomposite specifically for this working electrode. Then the anti-CD63 was immobilised on the MC-SPE/CNCs/Fe_3O_4/NAF surface to develop MC-SPE/CNCs/Fe_3O_4/NAF/anti-CD63. This revealed a slight decrease in the ECL signal due to quenching of tris (2,2′-bipyridyl) dichlororuthenium(II) activity over MC-SPE/CNCs/Fe_3O_4/NAF/anti-CD63 because of the formed insulating layer of anti-CD63, demonstrating the successful adsorption of the antibody layer [Fig. 6A, curve (c)]. Finally, MC-SPE/CNCs/Fe_3O_4/NAF/anti-CD63 nanosensor was incubated with 10 µL of 0.1 % blocking agent (BSA) to inhibit non-specific binding sites the electrode surface. ECL intensity further decreased due to further quenching of tris (2,2′-bipyridyl) dichlororuthenium(II) activity over MC-SPE/CNCs/Fe_3O_4/NAF/anti-CD63/BSA because of the formation of another insulating layer of BSA, portraying the adsorption of the BSA to form MC-SPE/CNCs/Fe_3O_4/NAF/anti-CD63/BSA nanoimmunosensor [Fig. 6A, curve (d)]. Further, surface charge was evaluated for each layer of the immunosensor using CC (Fig. 6B). The surface charge layer of the nanoimmunosensors displayed a correlation with the ECL intensity. Additionally, layer-by-layer characterisation studies were performed via EIS and CV, as shown in supplementary materials Fig. S2A and Fig. S2B, respectively.

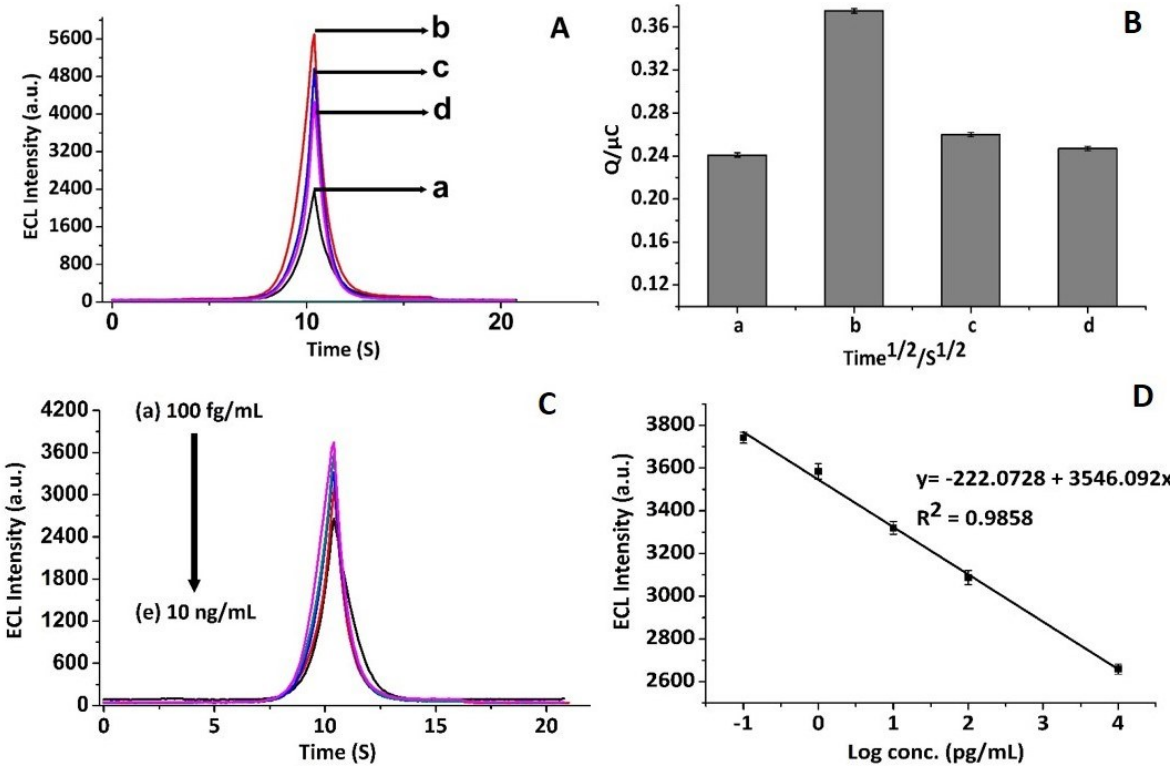

Fig. 6. Layer-by-layer characterisation, analytic performance, and diffusion kinetic analysis: **(A)** ECL intensity curve of: **(a)** MC-SPE, **(b)** MC-SPE/CNCs/Fe_3O_4/NAF, **(c)** MC-SPE/CNCs/Fe_3O_4/NAF/anti-CD63, **(d)** MC-SPE/CNCs/Fe_3O_4/NAF/anti-CD63/BSA/CD63 measured in luminophore solution, CSE = 100 mV/s using 1:100 $[Ru(bpy)_3]Cl_2$-TPrA solution containing 10 mM PBS, pH 7.4; **(B)** CC bar of: **(a)** MC-SPE, **(b)** MC-SPE/CNCs/Fe_3O_4/NAF, **(c)** MC-SPE/CNCs/Fe_3O_4/NAF/anti-CD63, **(d)** MC-SPE/CNCs/Fe_3O_4/NAF/anti-CD63/BSA/CD63, measured in redox probe (5 mM $[Fe(CN)_6]^{3-}$/$[Fe(CN)_6]^{4-}$) solution, CSE = 100 mV/s; **(C)** ECL dose response curves representing different concentrations of CD63 from 10 ng mL^{-1} to 100 fg mL^{-1}: **(a)** 100 fg mL^{-1}, **(b)** 100 pg mL^{-1}, **(c)** 10 pg mL^{-1}, **(d)** 1 pg mL^{-1}, **(e)** 10 ng mL^{-1}; **(D)** The calibration plot of the CD63 nanoimmunosensors towards different concentrations from 10 ng mL^{-1} to 100 fg mL^{-1} of CD63 (n=3).

3.10. Analytical performance of the fabricated nanoimmunosensor

To evaluate the analytical performance of our proposed immunosensor, the MC-SPE/CNCs/Fe_3O_4/NAF/anti-CD63/BSA platform was incubated with different concentrations (100 fg mL^{-1} to 10 ng mL^{-1}) of CD63 (Fig. 6C). A calibration plot was plotted using the log concentrations of the CD63 antigen, ranging from 100 fg mL^{-1} to 10 ng mL^{-1} against ECL intensity under optimum conditions (at 21 ± 0.5ºC in an air-conditioned laboratory, at 10 mM

PBS pH 7.4 using 100 mM $[Ru(bpy)_3]Cl_2$ 1 mM TPrA. The linearity graph (Fig. 6D) showed a negative linear relationship between the above-mentioned concentration range (100 fg mL^{-1} to 10 ng mL^{-1}; $R^2 = 0.9858$) and ECL intensity. This demonstrate that as the concentration of CD63 increases from 100 fg mL^{-1} to 10 ng mL^{-1} (Fig. 6C) over SPE/CNCs/Fe3O4/NAF/anti-CD63/BSA nanoimmunosensor quenching of tris (2,2′-bipyridyl) dichlororuthenium(II) activity over SPE/CNCs/Fe3O4/NAF/anti-CD63/BSA increases due to formed thick insulating layer of CD63 protein. Further, CD63 protein is slightly positively charged in the working pH (7.4) having a pI of 8.1 [38]. As a result of that, with increasing CD63 concentration, the ECL intensity faces a decreasing trend and vice versa (Fig. 6D). The limit of detection (LOD) for this study was found to be 100 fg mL^{-1}, which can be repeatedly detected by our CD63 specific immunosensor. The low LOD is due to the enhanced ECL activity and conductivity generated from the CNCs/Fe_3O_4/NAF nanocomposite [25, 28, 30, 32]. Besides, the large surface area of the MC-SPE with the enhanced electrochemical active area and enhanced electronic transfer properties also helped in quick electron transfer, and thus improve the overall performance of this fabricated immunosensor [41]. A comparison of different sensing strategies with designed immunosensor for CD63 detection has been presented in Table 1.

Detection Strategy	Method	Linearity	LOD	Reference
Electrochemical	RGO FET chip	0.5 μg mL^{-1} – 832.5 μg mL^{-1}	0.1 μg mL^{-1}	[42]
Electrochemical	CD63 aptamer immobilized gold electrode	10 μg mL^{-1} –1 μg mL^{-1}	1 μg mL^{-1}	[43]
Colourimetry	Aptamer-capped Fe_3O_4 NPs	100 μg mL^{-1} – 1.25 μg mL^{-1}	1.25 μg mL^{-1}	[44]
Fluorescence	Cy3-CD63 aptamer/Ti_3C_2 MXenes nanocomplex	100 μg mL^{-1} – 40 μg mL^{-1}	40 μg mL^{-1}	[45]
Plasmonic Biosensor (SPR)	BAF-TiN biosensor	4.29 μg mL^{-1} –1.75 μg mL^{-1}	1.75 μg mL^{-1}	[46]
Electrochemiluminescence	MC-SPE/CNCs/Fe_3O_4/NAF	100 fg mL^{-1} – 10 ng mL^{-1}	100 fg mL^{-1}	This work

Table 1: Comparison of different sensing strategies with designed immunosensor for CD63 detection.

3.11. Label-free detection principle

In this study, the label-free MC-SPE/CNCs/Fe_3O_4/NAF/anti-CD63/BSA was authenticated for its ability to detect 100 pg mL^{-1} CD63, which was recorded as ECL intensity plotted against time in supplementary materials Fig. S3A and shown by bars in supplementary materials Fig. S3B. The analytical efficiency of the proposed sensor was verified by the relative standard deviation (RSD %), less than 5% [47]. As, target protein (CD63) has an isoelectric point (pI) of 8.1 carrying positive charge at the working pH 7.4, repulsing the positively charged luminophore ($Ru(bpy)_3]Cl_2$) and co-reactant (TPrA) [48]. Consequently, the diffusion of $Ru(bpy)_3]Cl_2$-TPrA onto the immunocomplex was hindered with the increasing CD63

concentration resulting in a declined ECL signal. For additional validation that the ECL intensity is dependent on the $Ru(bpy)_3]Cl_2$-TPrA diffusion process. ECL study was performed (supplementary materials Fig. S2A) which showed that in the presence of the target protein, the total ECL intensity determined was condensed demonstrating that less $[Ru(bpy)_3]Cl_2$ was dispersed towards CD63 antigen.

3.12. Repeatability, stability, selectivity and cross-reactivity study

The reproducibility of the developed MC-SPE/CNCs/Fe_3O_4/NAF/anti-CD63/BSA nanoimmunosensor was examined by fabricating five electrodes at different times and later evaluating their respective signals. The concentrations of CD63 used for testing each electrode fabrication was 100 pg mL^{-1} (Fig. 7A). The proposed nanoimmunosensor showed significant reproducibility with a potential to clinical sample analysis to detect CD63 protein. Next, the stability of the fabricated immunosensor was calculated by storing four electrodes up to twelve days, having a time interval of four days (Fig. 7B). The electrodes showcased a gradual descending trend of signals upon storing at 4°C, demonstrating long term stability patterns. Following that, the selectivity of the MC-SPE/CNCs/Fe_3O_4/NAF/anti-CD63/BSA nanosensor was investigated. Two different types of exosomal proteins (CD69, CD81: concentration 100 pg mL^{-1}) were tested on fabricated MC-SPE/CNCs/Fe_3O_4/NAF/anti-CD63/BSA nanoimmunosensors. Thereafter, results were compared with 100 pg mL^{-1} of CD63 (Fig. 7C). Moreover, three more serum proteins CEA, AFP and Hp, were also tested for further confirmation of the selectivity performance of the proposed nanoimmunosensor (Fig. 7C). The results indicated the MC-SPE/CNCs/Fe_3O_4/NAF/anti-CD63/BSA nanoimmunosensors was extremely specific to our target proteins (CD63). Finally, for specificity study, the proposed nanoimmunosensor was tested with the mixture of non-target proteins for the real clinical sample analysis, and the signal was compared with CD63 (target protein) applying the same

working volume and concentration (Fig. 7D). All these data reassure the efficiency and potentiality of fabricated MC-SPE/CNCs/Fe_3O_4/NAF/anti-CD63/BSA nanoimmunosensor to detect CD63 protein to be used as a point-of care-testing device.

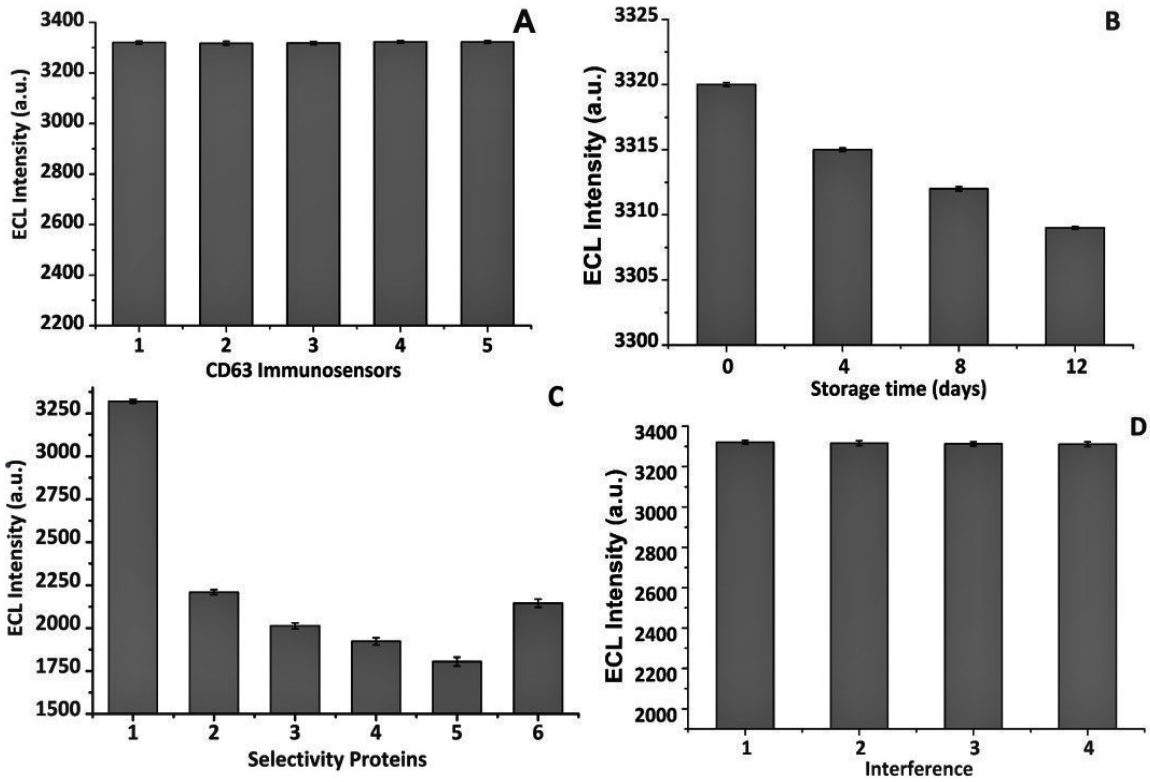

Fig. 7. Study of the reproducibility, stability, selectivity, and interference-resistance of the CD63 nanoimmunosensor: **(A)** Five fabricated MC-SPE/CNCs/Fe_3O_4/NAF/anti-CD63/BSA nanoimmunosensors were tested with 100 pg mL^{-1} CD63 and their signals were recorded; **(B)** MC-SPE/CNCs/Fe_3O_4/NAF/anti-CD63/BSA nanoimmunosensor stored at 4 °C and tested with 100 pg mL^{-1} CD63 at different five days interval; **(C)** CD63 nanoimmunosensor was tested against other analytes known to be present in serum and the signal was recorded. The different antigens tested were: (1) 100 pg mL^{-1} CD63; (2) 100 pg mL^{-1} CD69; (3) 100 pg mL^{-1} CD81, (4) 100 pg mL^{-1} CEA; (5) 100 pg mL^{-1} AFP; (6) 100 pg mL^{-1} Hp (n = 3); and **(D)** CD63 nanoimmunosensor was tested against 100 pg mL^{-1} of CD63 in combination with 100 pg mL^{-1} of other analytes known to be present in serum and the signal recorded. The antigen mixture tested were (1) CD63 only; (2) CD63 + CD69; (3) CD63 + CD81; (4) CD63 + CD69 + CD81 (n=3).

4. Conclusions

The important goal of this work was to detect CD63 protein in traces amount with good interference-resistance capacity. So detection limit of 100 fg mL^{-1} was observed for this MC-SPE/CNCs/Fe_3O_4/NAF/anti-CD63/BSA nanoimmunosensor with a wide linear range of 100 fg mL^{-1} to 10 ng mL^{-1}. This study demonstrates the capability of a new carbon nanomaterial, CNCs and its impact on detecting CD63. Both CNCs and Fe_3O_4 had been proven to highly accelerate ECL intensity over MC-SPE in optimal conditions. This fabricated immunosensor also showcased good reproducibility and specificity in real-time. We have certainly overcome the challenge of stability issues in the case of using new nanocomposite (CNCs/Fe_3O_4/NAF) in the ECL technique. In addition, the combination of $[Ru(bpy)_3]Cl_2 \cdot 6H_2O$) and TPrA as luminophore and co-reactant respectively could be applied to detect other clinically important proteins (e.g. CD69, CD81). However, the trend and versatility of our proposed nanocomposite (CNCs/Fe_3O_4/NAF) need to be evaluated with other biomarkers to make it more dynamic and open up multiplexed detection opportunities. Besides, the practicality of this proposed immunosensor needs to be further assessed in the future by culturing exosome specific cell lines and extracting-quantifying the target protein before finalizing this ECL nanoimmunosensor for real-world applications. Further, MC-SPE/CNCs/Fe_3O_4/NAF interface could be used to fabricate antigen-antibody based different rapid and sensitive testing devices.

Acknowledgements

Juthi Adhikari is grateful to the UBD's university graduate scholarship (UGS) for providing the financial support to pursue her Ph.D. degree. Dr. Mohammad Rizwan gratefully acknowledge CALIN and the Welsh European Funding Office (WEFO).

Funding

This work was partly supported by the Universiti Brunei Darussalam's grant UBD/RSCH/1.4/FICBF(b)/2020/025, along with Brunei Research Council [Grant# 4 and 10] of Negara Brunei Darussalam.

Conflict of interest

The authors declare no financial or commercial conflicts of interest.

Supplementary data

Supplementary data associated with this article can be found in the online version.

References

[1] Thomas, S.N.; Liao, Z.; Clark, D.; Chen, Y.; Samadani, R.; Mao, L.; Ann, D.K.; Baulch, J.E.; Shapiro, P.; Yang, A.J. Exosomal Proteome Profiling: A Potential Multi-Marker Cellular Phenotyping Tool to Characterize Hypoxia-Induced Radiation Resistance in Breast Cancer. *Proteomes*, **2013**, *1*, 87–108.

[2] Hartjes, T.A.; Mytnyk, S.; Jenster, G.W.; Van Steijn, V.; Van Royen, M.E. Extracellular Vesicle Quantification and Characterization: Common Methods and Emerging Approaches. *Bioengineering*, **2019**, *6*, 5-7.

[3] Jakobsen, K.R.; Paulsen, B.S.; Baek, R.; Varming, K.; Sorensen, B.S.; Jørgensen, M.M. Exosomal proteins as potential diagnostic markers in advanced non-small cell lung carcinoma. *J. Extracell. Vesicles*., **2015**, *4*, 26658–26659.

[4] Jung, K.K.; Liu, X.W.; Chirco, R.; Fridman, R.; Kim, H.R.C. Identification of CD63 as a tissue inhibitor of metalloproteinase-1 interacting cell surface protein. *The EMBO J*., **2006**, *25*, 3934–3942.

[5] Dogrammatzis, C.; Deschamps, T.; Kalamvoki, M. Biogenesis of Extracellular Vesicles during Herpes Simplex Virus 1 Infection: Role of the CD63 Tetraspanin. *J. Virol*., **2019**, *93*, 1850.

[6] Doldán, X.; Fagúndez, P.; Cayota, A.; Laíz, J.; Tosar, J.P. Electrochemical Sandwich Immunosensor for Determination of Exosomes Based on Surface Marker-Mediated Signal Amplification. *Anal. Chem*., **2016**, *88*, 10466−10473.

[7] Boriachek, K.; Islam, M.N.; Gopalan, V.; Lam, A.K.; Nguyen, N.T.; Shiddiky, M.J. Quantum dot-based sensitive detection of disease specific exosome in serum. *Analyst,* **2017**, *142*, 2211–2219.

[8] Campos-Silva, C.; Suárez, H.; Jara-Acevedo, R.; Linares-Espinós, E.; Martinez-Piñeiro, L.; Yáñez-Mó, M.; Valés-Gómez, M. High sensitivity detection of extracellular vesicles immunecaptured from urine by conventional flow cytometry. *Sci. Rep*., **2019**, *9*, 2042.

[9] Kowal, E.J.; Ter-Ovanesyan, D.; Regev, A.; Church, G.M. Extracellular Vesicle Isolation and Analysis by Western Blotting. *Methods Mol. Biol*., **2017**, *1660*, 143–152.

[10] Kilic, T.; Valinhas, A.T.D.S.; Wall, I.; Renaud, P.; Carrara, S. Label-free detection of hypoxiainduced extracellular vesicle secretion from MCF-7 cells. *Sci. Rep*., **2018**, *8*, 9402.

[11] Li, W.; Li, C.; Zhou, T.; Liu, X.; Liu, X.; Li, X.; Chen, D. Role of exosomal proteins in cancer diagnosis. *Mol. Cancer*. **2017**, *16*, 144–145.

[12] Rizwan, M.; Mohd-Naim, N.F.; Keasberry, N.A.; Ahmed, M.U. A highly sensitive and label-free electrochemiluminescence immunosensor for beta 2-microglobulin. *Anal. Methods*. **2017**, *9*, 2570–2577.

[13] Brown, K.; McMenemy, M.; Palmer, M.; Baker, M.J.; Robinson, D.W.; Allan, P.; Dennany, L. Utilization of an Electrochemiluminescence Sensor for Atropine Determination in Complex Matrices. *Anal. Chem.,* **2019**, *91*, 12369–12376.

[14] Bertoncello, P.; Stewart, A.J.; Dennany, L. Analytical Applications of Nanomaterials in Electrogenerated Chemiluminescence. *Anal. Bioanal. Chem.,* **2014**, *406*, 5573-5587.

[15] L., Dennany. Electrochemiluminescence fundamentals and analytical applications, In Electrochemistry: Ed. C. Banks, S. McIntosh, RSC, **2018**, *15*, 96 -146.

[16] Brown, K.; Stewart, A.J.; Dennany, L. Cathodic Quantum Dot Facilitated Electrochemiluminescent Detection in Blood. *Anal Chem*, **2018,** *90*, 12944-12950.

[17] Stewart, A.J.; Hendry, J.; Dennany, L. Whole Blood Electrochemiluminescent Detection of Dopamine. *Anal Chem*, **2015**, *87*, 11847-11853.

[18] Liu, Z.; Qi, W.; Xu, G. Recent advances in electrochemiluminescence. *Chem. Soc. Rev.*, **2015**, *44*, 3117-3142.

[19] Cui, H.; Paolucci, F.; Sojic, N.; Xu, G. Analytical electrochemiluminescence. *Anal. Bioanal. Chem.*, **2016**, *408*, 7001-7002.

[20] Gao, W.; Saqib, M.; Qi, L.; Zhang, W.; Xu, G. Recent advances in electrochemiluminescence devices for point-of-care testing. *Curr. Opin. Electrochem.,* **2017**, *3*, 4-10.

[21] Rizwan, M.; Mohd-Naim, N.F.; Ahmed, M.U. Trends and Advances in Electrochemiluminescence Nanobiosensors. *Sensors*, **2018**, *18*, 166.

[22] Rizwan, M.; Ahmed, M.U. Electrochemiluminescence study of AuNPs/CdTe-QDs/SWCNTs/chitosan nanocomposite modified carbon nanofiber screen-printed electrode with $[Ru(bpy)_3]^{2+}$/TPrA. *Inorg. Chem. Commun.,* **2019**, *106*, 54-60.

[23] Tang, Y.; Li, J.; Guo, Q.; Nie, G. An ultrasensitive electrochemiluminescence assay for Hg2+ through graphene quantum dots and poly (5-formylindole) nanocomposite. *Sens. Actuators B Chem.*, **2019**, *282*, 824–830.

[24] Lim S.A.; Yoshikawa, H.; Tamiya, E.; Yasin, H.M.; Ahmed, M.U. A highly sensitive gold nanoparticle bioprobe based electrochemical immunosensor using screen printed graphene biochip. *RSC Adv*., **2014**, *4*, 58460–58466.

[25] Rizwan, M.; Keasberry, N.A.; Ahmed, M.U. Efficient double electrochemiluminescence quenching based label-free highly sensitive detection of haptoglobin on a novel nanocomposite modified carbon nanofibers interface. *Sens. Biosensing Res*., **2019**, *24*, 100284.

[26] Ahmed, M.U.; Saaem, I.; Wu, P.C.; Brown, A.S. Personalized diagnostics and biosensors: a review of the biology and technology needed for personalized medicine. *Crit. Rev. Biotechnol*., **2014**, *34*, 180–196.

[27] Lim, S.A.; Ahmed, M.U. Electrochemical immunosensors and their recent nanomaterial-based signal amplification strategies: a review. *RSC Adv*., **2016**, *30*, 24995–25014.

[28] Singh, B.; Dempsey, E.; Laffir, F. Carbon nanochips and nanotubes decorated PtAuPd-based nanocomposites for glucose sensing: Role of support material and efficient Pt utilisation. *Sens. Actuators B Chem.*, **2014**, *205*, 401–410.

[29] Mohamad, A.; Rizwan, M.; Keasberry N.A.; Ahmed, M.U. Fabrication of label-free electrochemical food biosensor for the sensitive detection of ovalbumin on nanocomposite-modified graphene electrode. *Biointerface Res. Appl. Chem*., **2019**, *9*, 4655-4662.

[30] Sheng, W.; Xu, Q.; Chen, J.; Wang, H.; Ying, Z.; Gao, R.; Zheng, X.; Zhao, X. Electrochemical sensing of hydrogen peroxide using nitrogen-doped graphene/porous iron oxide nanorod composite. *Mater*., **2019**, *235*, 137–140.

[31] Adhikari, J.; Keasberry, N.A.; Mahadi, A.H.; Yoshikawa, H.; Tamiya, E.; Ahmed, M.U. An ultra-sensitive label-free electrochemiluminescence CKMB immunosensor using a novel nanocomposite-modified printed electrode. *RSC Adv.*, **2019**, ***9***, 34283-34292.

[32] Guo, C.; Sun, H.; Zhao, X.S. Myoglobin within graphene oxide sheets and Nafion composite films as highly sensitive biosensor. *Sens. Actuators B Chem.*, **2012**, *164*, 82-89.

[33] Li, H.; Chen J.; Han, S.; Niu, W.; Liu, X.; Xu, G. Electrochemiluminescence from tris (2, 2′-bipyridyl) ruthenium (II)–graphene–Nafion modified electrode. *Talanta,* **2009**, 79, 165–170.

[34] Roy, S.; Wei, S.X.; Ying, J.L.Z.; Safavieh, M.; Ahmed, M.U. A novel, sensitive and label-free loop-mediated isothermal amplification detection method for nucleic acids using luminophore dyes. *Biosens. Bioelectron*., **2016**, *86*, 346-352.

[35] Sharma, S.; Byrne, H.; O'Kennedy, R.J. Antibodies and antibody-derived analytical biosensors. *Essays Biochem.,* **2016**, *60*, 9-18.

[36] Bharath, G., Alhseinat, E., Ponpandian, N., Khan, M.A., Siddiqui, M.R., Ahmed, F., Alsharaeh, E.H. 2017. Development of adsorption and electrosorption techniques for removal of organic and inorganic pollutants from wastewater using novel magnetite/porous graphene-based nanocomposites. *Sep. Purif. Technol.*, **2017**, *188*, 206–218.

[37] Hwang, S.W., Umar, A., Dar, G.N., Kim, S.H., Badran, R.I. Synthesis and characterization of iron oxide nanoparticles for phenyl hydrazine sensor applications. *Sensor Lett*., **2014**, *12*, 97-101.

[38] Zou, Y.; Wang, H.; Shapiro, J.L.; Okamoto, C.T.; Brookes, S.J.; Lyngstadaas, S.P.; Snead, M.L.; Paine, M.L. Determination of protein regions responsible for interactions of amelogenin with CD63 and LAMP1. *Biochem. J*., **2007**, *408*, 347–354.

[39] Okuno, J.; Maehashi, K.; Kerman, Y.; Takamura, K.; Matsumoto, K.; Tamiya, E. Label-free immunosensor for prostate-specific antigen based on single-walled carbon nanotube array-modified microelectrodes. *Biosens. Bioelectron*., **2007**, *22*, 2377–2381.

[40] Aydin E.B.; Aydin M.; Sezgintürk M.K. Electrochemical immunosensor based on chitosan/conductive carbon black composite modified disposable ITO electrode: An analytical platform for p53 detection. *Biosens. Bioelectron*., **2018**, *121*, 80–89.

[41] Wu, B.; Miao, C.; Yu, L.; Wang, Z.; Huang, C.; Jia. N. Sensitive electrochemiluminescence sensor based on ordered mesoporous carbon composite film for dopamine. *Sens. Actuators B Chem*., **2014**, *195*, 22–27.

[42] Yu, Y.; Li, Y.T.; Jin, D.; Yang, F.; Wu, D.; Xiao, M.M.; Zhang, H.; Zhang, Z.Y.; Zhang, G.J. Electrical and label-free quantification of exosomes with a reduced graphene oxide field effect transistor biosensor. *Anal. Chem.,* **2019**, *91*, 10679–10686.

[43] Qiu, G., Thakur, A., Xu, C., Ng, S.P., Lee, Y. and Wu, C.M.L. Detection of Glioma-Derived Exosomes with the Biotinylated Antibody-Functionalized Titanium Nitride Plasmonic Biosensor. *Adv. Funct. Mater.*, **2019**, *29*, 1806761.

[44] Zhou, Q.; Rahimian, A.; Son, K.; Shin, D.S.; Patel, T.; Revzin, A. 2016. Development of an aptasensor for electrochemical detection of exosomes. *Methods*, **2016**, *97*, 88–93.

[45] Zhang, Q.; Wang, F.; Zhang, H.; Zhang, Y.; Liu, M.; Liu, Y. Universal Ti_3C_2 MXenes based self-standard ratiometric fluorescence resonance energy transfer platform for highly sensitive detection of exosomes. *Anal. Chem.*, **2018**, *90*, 12737–12744.

[46] Chen, J.; Xu, Y.; Lu, Y.; Xing, W. Isolation and visible detection of tumor-derived exosomes from plasma. *Anal. Chem.*, **2018**, *90*, 14207–14215.

[47] Fu, Z.; Lu, Y.C.; Lai, J.J. Recent Advances in Biosensors for Nucleic Acid and Exosome Detection. *Chonnam. Med. J*., **2019**, 55, 86-98.

[48] Wusimanjiang, Y.; Meyer, A.; Lu, L.; Miao, W. Effects of multi-walled carbon nanotubes on the electrogenerated chemiluminescence and fluorescence of CdTe quantum dots. *Anal. Bioanal. Chem*., **2016**, *48*, 7049-7057.